Lawrence Berkeley National Laboratory

Title
Comparison of reactions for the production of 258,257Db: 208Pb(51V,xn) and 209Bi(50Ti,xn)

Permalink
https://escholarship.org/uc/item/45z1x7gc

Author
Gates, Jacklyn M.

Publication Date
2008-11-25

Comparison of reactions for the production of ^{258,257}Db: ^{208}Pb(^{51}V,xn) and ^{209}Bi(^{50}Ti,xn)

J.M. Gates[1,2], S.L. Nelson[1,2], K.E. Gregorich[1], I. Dragojević[1,2], Ch.E. Düllmann[1,2,*],

P.A. Ellison[1,2], C.M. Folden III[1,2,†], M.A. Garcia[1,2], L. Stavsetra[1], R. Sudowe[1,‡],

D.C. Hoffman[1,2], H. Nitsche[1,2]

[1] *Nuclear Science Division, Lawrence Berkeley National Laboratory, Berkeley, CA 9472, USA*

[2] *University of California, Berkeley, Berkeley, CA 94720, USA*

Abstract

Excitation functions for the 1n and 2n exit channels of the ^{208}Pb(^{51}V,xn)$^{259-x}$Db reaction were measured. A maximum cross section of the 1n exit channel of 2070^{+1100}_{-760} pb was measured at an excitation energy of 16.0 ± 1.8 MeV. For the 2n exit channel, a maximum cross section of 1660^{+450}_{-370} pb was measured at 22.0 ± 1.8 MeV excitation energy. The 1n excitation function for the ^{209}Bi(^{50}Ti,n)^{258}Db reaction was remeasured, resulting in a cross section of 5480^{+1730}_{-1370} pb at an excitation energy of 16.0 ± 1.6 MeV, in agreement with previous values [F. P. Heßberger, *et al.*, Eur. Phys. J. A **12**, 57 (2001)]. Differences in cross section maxima are discussed in terms of the fusion probability below the barrier.

PACS numbers: 25.70.Gh, 27.90.+b, 23.60.+e

I. INTRODUCTION

Neutron-deficient isotopes of elements 104 - 113 have been produced in 'cold' nuclear fusion reactions with ^{208}Pb and ^{209}Bi targets and stable projectiles from Ti to Zn [1-6]. In these reactions, the compound nucleus is formed at excitation energies as low as 10 - 15 MeV, hence 'cold' fusion. These low excitation energies allow for de-excitation of the compound nucleus by the evaporation of only one neutron (apart from γ-ray emission).

Recently, Świątecki *et al.* have developed the Fusion by Diffusion (FBD) model for predicting cold fusion reaction cross sections [7, 8]. According to the FBD model, the cross section is a product of three terms: i) the probability, σ_{cap}, for the target and projectile to become captured in a pocket of their mutual coulomb + nuclear potential, thus forming a composite system, ii) the probability, P_{CN}, for this composite system to form a compound nucleus, iii) the probability, $\dfrac{\Gamma_n}{\Gamma_t}$, for the compound nucleus to de-excite by the emission of one neutron in competition with all other de-excitation modes (predominantly fission) times the probability, $P_<$, that after evaporation of the first neutron, the nucleus is below the thresholds for second chance fission and additional neutron evaporation. The total cross section is then given by:

$$\sigma_{tot} = \sigma_{cap} \times P_{CN} \times \frac{\Gamma_n}{\Gamma_t} P_< \tag{1}$$

To test this model, the 1*n* excitation functions of coupled reaction pairs have been studied [6, 9, 10]. In these coupled reaction pairs, an odd proton is contained in the projectile of the first reaction, resulting in an e-e target and an o-e projectile. For the second reaction, the odd proton moved to the target yielding an o-e target and an e-e

projectile (e.g. the $^{208}_{82}Pb(^{51}_{23}V,n)$ and $^{209}_{83}Bi(^{50}_{22}Ti,n)$ reactions). As the same compound

nucleus is produced in both reactions, the last term in the FBD model, $\frac{\Gamma_n}{\Gamma_{tot}}P_<$, is identical

for the two reactions (ignoring small differences in angular momentum), allowing for the

investigation of the product of σ_{cap} and P_{CN}. For two similar reactions, P_{CN} is expected to

be similar. However, the more asymmetric target-projectile combinations have smaller

repulsive Coulomb forces, which are expected to result in larger evaporation residue

(EVR) cross sections because of the larger σ_{cap} [7, 8].

Here we report on the measurement of the 1n and 2n excitation functions for the

$^{208}Pb(^{51}V,xn)^{259-x}Db$ reaction. The complementary reaction, $^{209}Bi(^{50}Ti,xn)^{259-x}Db$, was

studied earlier at the Gesellschaft für Schwerionenforschung (GSI) by Heßberger *et al*.

[11, 12]. We have also remeasured the 1n excitation function for the $^{209}Bi(^{50}Ti,n)^{258}Db$

reaction using a detection setup that was identical to the one used for the

$^{208}Pb(^{51}V,xn)^{259-x}Db$ reaction.

II. EXPERIMENTAL TECHNIQUE

Beams of $^{51}V^{11+}$ and $^{50}Ti^{12+}$ were accelerated to energies of $4.7-5.1$

MeV/nucleon in the Lawrence Berkeley National Laboratory's (LBNL) 88-Inch

Cyclotron. Typical beam intensities were 0.3 to 0.8 particle-μA [(1.8-5.0)·10^{12} s^{-1}]. At

the entrance to the Berkeley Gas-filled Separator (BGS) [13-15], the beam passed

through a 45-μg/cm^2 thick carbon (C) window that serves to separate the vacuum of the

beam line from the 67-Pa helium (He) gas inside the BGS. Nine arc-shaped target

segments were mounted on the circumference of a 35.6-cm diameter wheel which was

rotating at ~600 rpm and was located approximately one centimeter downstream of the

entrance window. For the irradiations with ^{51}V, each target segment consisted of ~470-μg/cm^2 metallic lead (98.4% ^{208}Pb, 1.1% ^{207}Pb and 0.5% ^{206}Pb) deposited on a 35-μg/cm^2 ^{nat}C backing and covered with 5-10 μg/cm^2 ^{nat}C. The energy thickness of the lead (Pb) layer on each target segment was approximately 4.5 MeV. Targets consisting of ~441-μg/cm^2 ^{209}Bi on a 35-μg/cm^2 ^{nat}C backing were irradiated with ^{50}Ti and had an energy thickness of ~3.9 MeV. Energy losses of ^{51}V through C and Pb and of ^{50}Ti through C and Bi were calculated with SRIM2006.02 [16].

Systematic uncertainty in the absolute energy from the 88-Inch Cyclotron is estimated to be ~1% [14]. Two PIN diode detectors located at ±27° from the beam axis monitored the product of target thickness and beam intensity on-line by the detection of Rutherford-scattered particles. Analysis of the pulse heights of the Rutherford-scattered projectiles provided relative energies to within 0.1% for the various ^{51}V and ^{50}Ti beam energies. These resulted in ^{51}V center-of-target (COT) beam energies of 236.1, 239.7, 244.1, 247.2, 250.8 and 255.0 MeV, while the ^{50}Ti COT beam energies were 229.5, 231.8, 233.6, 236.0 and 238.4 MeV. Compound nucleus excitation energies were calculated using these beam energies with the experimental mass defects for ^{51}V, ^{50}Ti, ^{208}Pb and ^{209}Bi [17] and the Thomas-Fermi mass defects (which include shell effects) for the compound nucleus [18]. The resulting ranges of compound nucleus excitation energies within the ^{208}Pb targets were 13.1 ± 1.8, 16.0 ± 1.8, 19.5 ± 1.8, 22.0 ± 1.8, 24.9 ± 1.8 and 28.3 ± 1.8 MeV. The ranges of compound nucleus excitation energies within the ^{209}Bi targets were 13.1 ± 1.6, 15.0 ± 1.6, 16.4 ± 1.6, 18.3 ± 1.6 and 20.6 ± 1.6 MeV.

Dubnium compound nucleus EVRs are formed with the momentum of the projectile and recoil from the target. These EVRs were separated from the beam and other unwanted reaction products in the BGS based upon their differing magnetic rigidities in He gas. Magnetic rigidities of the dubnium EVRs were estimated as previously described [14]. The efficiency for collecting dubnium EVRs at the BGS focal plane was modeled using a Monte Carlo simulation of the EVR trajectories in the BGS, as described earlier [14, 15], and resulted in energy dependent efficiencies, ε_{BGS}, of 53 – 58% and 66 – 70% for the $^{208}Pb(^{51}V,xn)$ and $^{209}Bi(^{50}Ti,xn)$ reactions, respectively. Between the $^{208}Pb(^{51}V,xn)$ and the $^{209}Bi(^{50}Ti,xn)$ experiments, a collimator upstream of the target was modified to decrease the vertical and increase the horizontal extension of the beam spot on the target wheel. The vertical magnification of reaction products in the BGS is a factor of -7. By decreasing the height of the collimator, the vertical distribution of the reaction products is smaller at the focal plane, and this resulted in an increased ε_{BGS} for the $^{209}Bi(^{50}Ti,xn)$ reaction.

After separation in the BGS, the dubnium recoils passed through a multi-wire proportional counter (MWPC) and were implanted into a focal plane detector (FPD). The MWPC was located ~23 cm upstream of the FPD and consisted of two 0.9-μm thick Mylar windows isolating an isobutane fill gas from the He of the BGS. The isobutane was held at a pressure of 0.5 kPa above the BGS pressure. An EVR passing through the MWPC (biased at +400-500 V) initiated a process of charge multiplication that was collected by electrodes at the top, bottom, left and right sides of the MWPC. A signal in the MWPC started the time-to-amplitude (TAC) converter that was stopped with a signal

in the FPD. This TAC signal between the MWPC and the FPD allowed for differentiation between implantation events and decays within the FPD.

The FPD was composed of an implantation detector and an upstream detector [6, 14]. The implantation detector consisted of 3 silicon cards, each containing 16 vertical strips that allowed for determination of the horizontal position. Energy was calibrated using a four-point α source containing ^{148}Gd, ^{239}Pu, ^{241}Am and ^{244}Cm. The α lines had a FWHM of 70 keV. The vertical position was determined by resistive charge division of the charges collected at the top and bottom of each strip [19]. Position resolutions were calculated using standard error propagation methods and are nearly proportion to 1/Energy. At the 1σ level, position resolutions were 0.24 – 0.35 mm over 9.4 – 7.0 MeV.

To discriminate decay-like events (events anti-coincident with a signal from the MWPC) from signals due to light and low-ionizing particles, which deposit a similar amount of energy in the FPD, three silicon cards were mounted directly behind the implantation detector. A signal in any of the 'punch-through' detector strips indicates light and low-ionizing particles.

Eight additional silicon cards were mounted perpendicular to, and upstream of, the implantation detector. These 'upstream' detectors allowed for greater efficiency in detecting α particles and spontaneous fission (SF) fragments escaping from the implantation detector. The efficiency for detecting α particles was ~76% of 4π: 51% of all α particles deposit their full energy in the implantation detector. An additional 25% of α particles lose a fraction of their energy in the focal plane detector and hit an upstream detector. Their full energy can thus be reconstructed by summing the signals in both the implantation and upstream detectors [hereafter, all events depositing their full

energy in the FPD (implantation detector only or split between the implantation and upstream detectors) are referred to as "full energy α's"]. Of the remaining 24% of all α particles, 16% escape out of the front of the detector box at an angle nearly normal to the focal plane, depositing less than 300 keV in the focal plane detector. As the deposited energy necessary to trigger the Multi-Branch System (MBS) data acquisition system [20] ranges from 200 keV at the top and bottom of the strips to 500 keV at the center, no information was recorded for ~16% of α-decays. Finally, about 8% of all α particles escape out of the front of the detector box but lose sufficient energy to trigger the data acquisition system (hereafter, such events are referred to as "escape α's").

Due to similarities in α-particle energies and lifetimes of ^{258,257}Db and their daughters, the rate of random escape-like events and the probability of not observing α particles, stringent rules were used to assign events to ^{258}Db or ^{257}Db. Assignment of a decay chain to ^{258}Db was made based on the observation of an EVR [$10.0 \leq E(MeV) \leq 30.0$, prompt TOF signal between MWPC and FPD, anti-coincident with punch-through and upstream detectors] correlated in position (same strip, $\pm 3\sigma$ vertical position) and time to either:

i) ^{258}Db-like α particles [$8.8 \leq E(MeV) \leq 9.4$, < 25 s]   followed by time- and position-correlated α particles of ^{254}Lr [$8.3 \leq E(MeV) \leq 8.6$, < 75 s].

ii) ^{258}Db-like α particles [$8.8 \leq E(MeV) \leq 9.4$, <25 s] followed by time- and position-correlated α particles of both ^{254}No [$8.0 \leq E(MeV) \leq 8.2$, < 325 s] and ^{250}Fm [$7.3 \leq E(MeV) \leq 7.6$, < 2 hr].

iii) ^{254}Lr-like α particles [8.3 ≤ E(MeV) ≤ 8.6, < 100 s] followed by time- and position-correlated α particles of ^{250}Md [7.6 ≤ E(MeV) ≤ 8.0, < 300 s].   In this case, the decay of ^{258}Db was assumed to go unobserved.

The α-decay of the electron capture (EC) daughter of ^{258}Db has recently been observed [21], however, due to similar decay properties, α-decay of ^{258}Db cannot be distinguished from α-decay of ^{258}Rf in chains that proceed through ^{254}No. At beam energies below the 2n exit channel threshold of 14.3 MeV, an EVR correlated in time (< 25 s) and position (same strip, ±3σ vertical position) to a spontaneous fission (SF) was also assigned to the decay of ^{258}Db. The detection of ^{250}Fm in case (iii) was also not required at beam energies below the 2n exit channel threshold.

^{257}Db was identified by the observation of an EVR [10.0 ≤ E(MeV) ≤ 30.0, anti-coincident with punch-through and upstream detectors, prompt TOF signal between MWPC and focal plane detector] followed by a time and position (same strip, ±3σ vertical position) correlated

i) ^{257}Db-like α particle [8.8 ≤ E(MeV) ≤ 9.4, < 10 s]   followed by a time- and position-correlated α or SF decay of ^{253}Lr [8.6 ≤ E$_α$(MeV) ≤ 8.9 or 100 ≤ E$_{SF}$(MeV) ≤ 300, < 10 s].

ii) ^{257}Db-like α particle [8.8 ≤ E(MeV) ≤ 9.4, < 10 s]   followed by time- and position-correlated α particles of both ^{249}Md [7.9 ≤ E(MeV) ≤ 8.2, < 325 s] and ^{245}Es [7.3 ≤ E(MeV) ≤ 7.6, < 500 s].

iii) ^{253}Lr-like α particle [8.6 ≤ E$_α$(MeV) ≤ 8.9, < 20 s] followed by the time- and position-correlated decay of either ^{249}Md [7.9 ≤ E(MeV) ≤ 8.2, < 150 s] or ^{245}Es

$[7.6 \leq E(\text{MeV}) \leq 7.8, \ < 500 \text{ s}]$. The decay of ^{257}Db was assumed to go unobserved in this case.

Events identified as α particles were required to be anti-coincident with the MWPC and punch-through detectors, in the same strip as and within a vertical position of $\pm 3\sigma$ of the EVR.

To minimize the contribution of random correlation of unrelated events, a fast beam-shutoff scheme was employed. Upon the detection of an EVR-like event followed by a position- (same strip, ± 3 mm vertical position) and time-correlated (< 180 s) α-like event $[8.0 \leq E(\text{MeV}) \leq 10.0]$, the beam was shutoff for 240 s to allow for detection of additional α- or SF-like events under nearly background-free conditions. This fast shutoff mode was employed for all energies of both reactions except the 236.1 and 244.1 MeV ^{51}V irradiations.

III. RESULTS

The spectrum of all focal plane events with $6 < E(\text{MeV}) < 10$ in the high-gain ADCs (anti-coincident with the MWPC and punch-through detector) is presented in Fig. 1a. The spectrum of all α-like events initiating a beam shutoff is contained in Fig. 1b, while Fig. 1c shows all α-like events occurring during the beam shutoff and correlated in time (<240 s) and position (same strip, $\pm 3\sigma$ vertical position) to the α-like event initiating beam shutoff. Fig. 1d shows all α-like events occurring during the beam off that were *not* correlated in time (<240 s) and position (same strip, $\pm 3\sigma$ vertical position) to the α-like event initiating beam shutoff. Tables I and II contain the beam energies, excitation energies, BGS efficiency, number of events observed and cross sections for the ^{208}Pb(^{51}V,xn)$^{259-x}$Db and ^{209}Pb(^{50}Ti,xn)$^{258-x}$Db reactions, respectively.

A. ^{258}Db

68 α-decay chains observed in the two reactions were attributed to the decay of ^{258}Db. 9 EVR-SF correlations were observed at the lowest two ^{50}Ti beam energies. The SF events were attributed to decay of ^{258}Rf, the electron capture (EC) daughter of ^{258}Db, as the excitation energy of the compound nucleus was at least 2 MeV below the threshold for the 2n exit channel. The half-life measured from the 77 observed decays of ^{258}Db is $4.2^{+0.4}_{-0.3}$ s, in agreement with the accepted value of 4.5 ± 0.6 s [17]. The half-life measured for the ^{254}Lr daughter is $17.8^{+1.9}_{-1.6}$ s, that for the ^{250}Md granddaughter is $24.7^{+9.5}_{-5.4}$ s and the measured half-life of the ^{250}Fm great-granddaughter is $28.4^{+3.9}_{-3.0}$ min. The values for ^{254}Lr and ^{250}Fm are in good agreement with the accepted values of 13 ± 3 s and 30 ± 3 min, respectively [17]. The measured half-life of ^{250}Md is shorter than accepted values of 52 ± 6 s [17].   The average magnetic rigidity measured for the ^{258}Db EVRs was 2.17 ± 0.01 T·m.

B. ^{257}Db

48 decay chains observed during the two reactions were attributed to the α-decay of ^{257}Db. Of these, 44 were followed by the detection of a full energy α particle of ^{253}Lr. ^{257}Db and ^{253}Lr are both known to have a ground and isomeric state with differing α-decay energies and lifetimes [12]. In this work, ^{257}Db and ^{253}Lr decays were assigned to the decay of the ground or metastable states based upon measured α-particle energies. The resulting half-lives of the ground and isomeric states of ^{257}Db are $1.82^{+0.27}_{-0.21}$ s and $0.58^{+0.13}_{-0.09}$ s, respectively, and $0.80^{+0.19}_{-0.13}$ s and $1.60^{+0.24}_{-0.18}$ s for the ground and isomeric states, respectively, of ^{253}Lr. These values are in agreement with accepted data [12, 17]. The half-life measured for the ^{249}Md granddaughter is $23.8^{+3.8}_{-2.9}$ s, and that for the ^{245}Es great-

granddaughter is $0.92^{+0.20}_{-0.14}$ min, consistent with the accepted values of 24 ± 4 s and 1.1 ± 0.1 min, respectively [17]. The average magnetic rigidity of the [257]Db EVRs was measured for the reactions and determined to be 2.15 ± 0.02 T·m.

C.   Random Rates

EVR-α-α (EVR-α-SF) random rates were calculated by multiplying the observed number of EVRs with the probability of observing two α particles (or correlated α-SF) within the required time and position windows. The rate of EVR-like events in the focal plane detector was $0.2 - 0.04$ s^{-1}, while the rate of α-like events was $(7-11) \cdot 10^{-3}$ s^{-1}. 71 high energy SF-like events (>100 MeV, anti-coincident with MWPC and punch-through detectors) were observed during the irradiation. A variety if different EVR-α-α decay parameters were used for identification of [258,257]Db. The highest number of random correlations was expected for identification of [258]Db via scenario ii. 0.05 random correlations of this type were expected during the irradiation, thus, it is unlikely that any of the α-decay chains are of random origin. Identification of [257]Db from EVR-α-SF correlations required detection of time and position correlated EVR, α, and SF events. The number of expected randomly occurring decay chains fitting the prescribed parameters is 2×10^{-5}.

Random rates for EVR-SF correlations were calculated by multiplying the observed number of SF events with the probability of observing an EVR preceding the SF within the predefined time and position windows. EVR-SF correlations were assigned to the decay of [258]Db at the lowest [51]V beam energy and two lowest [50]Ti beam energies, where the excitation energy of the compound nucleus was below the threshold for the 2n exit channel. During the irradiations at these energies, 16 SF-like events

[100 < E(MeV) < 300, anti-coincident with MWPC and punch-through detectors] were observed. Nine of them were correlated to EVRs recorded in the same strip within 25 s and a position window of ± 3σ. Based on the rate of EVR-like events, 0.3 random correlations were expected, and it is thus unlikely that more than one of the nine observed EVR-SF correlations is of random origin.

D.   Excitation Functions

To determine maximum cross sections, the excitation functions were fit using a method described in [22, 23]. The shape of the excitation function was modeled with a Gaussian on the low-energy side smoothly joined to an exponential on the high-energy side using:

$$\sigma = \sigma_{max}e^{-(E^*-c)^2/2w^2}, E^* \leq \lambda w^2 + c \tag{2}$$

$$\sigma = \sigma_{max}e^{\lambda^2 w^2/2}e^{-\lambda(E^*-c)}, E^* > \lambda w^2 + c$$

where E^* is the excitation energy, $-\lambda$ is the slope of the exponential and σ_{max} is the amplitude of the Gaussian with a centriod c and a width w.

Fig. 2 shows excitation functions of the 1n and 2n exit channels of the ^{208}Pb(^{51}V,xn) reaction. Horizontal error bars represent the range of beam energies covered inside the target, while vertical error bars represent the uncertainties due to counting statistics and are presented at the 1σ level [24]. A fit to the 1n data indicates that the excitation function has a maximum cross section of 2160 ± 530 pb at 15.2 ± 0.9 MeV. The maximum cross section of the 2n exit channel occurs at 23.4 ± 1.0 MeV and is 1980 ± 300 pb, nearly equal to that of the 1n exit channel.

The 1n excitation function for the ^{209}Bi(^{50}Ti,xn) reaction, as well as the 2n cross sections at the two highest ^{50}Ti beam energies are shown in Fig. 3. The maximum cross

section of 5910 ± 810 pb occurs at an excitation energy of 16.2 ± 0.6 MeV for the 1n exit

channel. These results are slightly higher than the previous value of 4300 ± 400 pb at

15.8 ± 0.1 MeV obtained by Heßberger *et al.* [12]. In [12] a value of 2400 ± 300 pb is

given as the maximum of the 2n cross section, approximately half that of the 1n exit

channel.

Fig. 3 also includes the 1n excitation function measured by Heßberger *et al.* in

[12, 25]. The cross sections for the data from [12, 25][1] were plotted using excitation

energies calculated from experimental mass defects for ^{50}Ti and ^{209}Bi [17] and the

Thomas-Fermi mass defects (which include shell effects) for the compound nucleus [18],

so that all excitation energies in this work are calculated in a consistent way. Based on

the differences between the ^{209}Bi(^{50}Ti,1n) excitation function measured in this work and

in [12, 25], an energy discrepancy of several MeV may exist between beam energies

reported in the two experiments.

IV. DISCUSSION

A comparison of the excitation functions for the 1n exit channels of the

^{208}Pb(^{51}V,xn) and ^{209}Bi(^{50}Ti,xn) reactions is shown in Fig. 4. The maximum cross section

for the ^{209}Bi(^{50}Ti,xn) reaction is 2.7 ± 1.1 times larger than the maximum ^{208}Pb(^{51}V,xn)

cross section. According to the FBD model, location of the maximum of the 1n

excitation function is a result of competition between two factors that vary with energy:

the reaction channel for single neutron emission, $\sigma_{cap} \times P_{CN} \times \dfrac{\Gamma_n}{\Gamma_t}$, and losses in EVR

formation due to second chance fission or neutron emission, $P_<$. The reaction channel for

single neutron emission increases with increasing bombarding energy, however, $P_<$

decreases with increasing energy once the threshold for second chance fission or neutron

emission has been reached [7, 8]. Since the threshold for $P_<$ depends on the compound

nucleus and not the method of formation, the energy at which the maximum cross

sections of the $1n$ exit channels is located is expected to be similar for the two reactions.

This is in agreement with our result that the maximum cross sections occur at excitation

energies of 15.2 ± 0.7 and 16.2 ± 0.6 MeV, for the ^{208}Pb(^{51}V,xn) and ^{209}Bi(^{50}Ti,xn)

reactions, respectively.

For two reactions that produce the same compound nucleus, losses in EVR

formation due to $\dfrac{\Gamma_n}{\Gamma_{tot}} P_<$ are the almost identical, and losses due to P_{CN} are expected to be

similar for two nearly identical reactions [7, 8]. Prior to forming a compound nucleus,

the nuclei must first overcome a barrier formed from their mutual coulomb + nuclear

potential [8]. The barrier heights as calculated using eqn. (5) in [8] are 251.9 MeV and

242.4 MeV in laboratory frame for the ^{208}Pb(^{51}V,n) and ^{209}Bi(^{50}Ti,n) reactions,

respectively. These correspond to respective excitation energies of 25.8 and 23.4 MeV.

The effect of this difference in σ_{cap} as a function of energy is shown in Fig. 4.

Comparison of the experimental excitation functions at low energies is hindered by

counting statistics, as only one event was observed for each reaction. Above the peak,

the ^{208}Pb(^{51}V,n) reaction has consistently lower experimental cross sections than the

^{209}Bi(^{50}Ti,n) reaction, an effect mirrored in the ratio of calculated σ_{cap} values for the two

reactions. Differences in experimental ^{208}Pb(^{51}V,n) and ^{209}Bi(^{50}Ti,n) cross sections

appear to be mainly due to the difference in capture cross sections for the two reactions.

Fig. 5 shows a comparison of the experimental excitation functions for the

^{208}Pb(^{51}V,2n) (this work) and ^{209}Bi(^{50}Ti,2n) [12, 25] reactions and includes σ_{cap} as a

function of energy. Due to possible energy discrepancies between the two laboratories,

direct comparison of the 2n cross sections is difficult. However, over the energy range of the excitation functions, σ_{cap} is larger for the ^{209}Bi(^{50}Ti,2n), again due to the height of the barrier in relation to the excitation energy of the compound nucleus. From this the maximum cross section for the ^{209}Bi(^{50}Ti,2n) should be larger than that of the ^{208}Pb(^{51}V,2n) reaction, however, the maximum cross sections of the two reactions are identical within the error bars.

IV. CONCLUSION

We have measured the 1n and 2n excitation functions for the ^{208}Pb(^{51}V,xn)$^{259-x}$Db reaction and re-measured the 1n excitation function for the ^{209}Bi(^{50}Ti,n)^{258}Db reaction. The maximum cross section of the ^{209}Bi(^{50}Ti,n) reaction is larger than the maximum of the ^{208}Pb(^{51}V,n) reaction. The FBD model suggests that these differences are due to the effect of the height of the barrier on σ_{cap}.

[*] Present address: Abteilung Kernchemie, Gesellschaft für Schwerionenforschung mbH, 64291 Darmstadt, Germany

[†] Present address: National Superconducting Cyclotron Laboratory, Michigan State University, East Lansing, MI 48824, USA

‡ Present address: Department of Health Physics, University of Nevada, Las Vegas, Las

Vegas, NV 89154, USA

[1] In the mass tables used in Ref. [12] [Audi *et al.*, Nuc. Phys. **A624**, 1 (1997)], element

105 is referred to with the symbol "Jl"; "Db" is used for element 104.

[1]   S. Hofmann, Rep. Prog. Phys. **61**, 639 (1998).
[2]   S. Hofmann and G. Münzenberg, Rev. Modern Phys. **72**, 733 (2000).
[3]   S. Hofmann*, et al.*, Eur. Phys. J. A **14**, 147 (2002).
[4]   K. Morita*, et al.*, J. Phys. Soc. Japan **76**, 043201 (2007).
[5]   K. Morita*, et al.*, J. Phys. Soc. Japan **73**, 2593 (2004).
[6]   C. M. Folden III, K. E. Gregorich, Ch. E. Düllmann, H. Mahmud, G. K. Pang, J. M. Schwantes, R. Sudowe, P. M. Zielinski, H. Nitsche, and D. C. Hoffman, Phys. Rev. Lett. **93**, 212702 (2004).
[7]   W. J. Świątecki, K. Siwek-Wilczyńska, and J. Wilczyński, Acta Phys. Pol. B **34**, 2049 (2003).
[8]   W. J. Świątecki, K. Siwek-Wilczyńska, and J. Wilczyński, Phys. Rev. C **71**, 014602 (2005).
[9]   C. M. Folden III, S. L. Nelson, Ch. E. Düllmann, J. M. Schwantes, R. Sudowe, P. M. Zielinski, K. E. Gregorich, H. Nitsche, and D. C. Hoffman, Phys. Rev. C **73**, 014611 (2006).
[10]   S. L. Nelson, C. M. Folden III, K. E. Gregorich, I. Dragojević, Ch. E. Düllmann, R. Eichler, M. A. Garcia, J. M. Gates, R. Sudowe, and H. Nitsche, (unpublished).
[11]   F. P. Heßberger*, et al.*, Z. Phys. A **322**, 557 (1985).
[12]   F. P. Heßberger*, et al.*, Eur. Phys. J. A **12**, 57 (2001).
[13]   W. Loveland, K. E. Gregorich, J. B. Patin, D. Peterson, C. Rouki, P. M. Zielinski, and K. Aleklett, Phys. Rev. C **66**, 044617 (2002).
[14]   K. E. Gregorich*, et al.*, Phys. Rev. C **72**, 014605 (2005).
[15]   K. E. Gregorich*, et al.*, Eur. Phys. J. A **18**, 633 (2003).
[16]   J. F. Ziegler, Nucl. Instrum. Methods B **219-220**, 1027 (2004).
[17]   G. Audi, O. Bersillon, J. Blachot, and A. H. Wapstra, Nucl. Phys. **A729**, 3 (2003).
[18]   W. D. Myers and W. J. Świątecki, Lawrence Berkeley National Laboratory Report; LBNL-36803 (1994); http://ie.lbl.gov/txt/ms.txt.
[19]   J. L. Alberi and V. Radeka, IEEE Trans. Nucl. Sci. **23**, 251 (1976).
[20]   H. G. Essel and N. Kurz, IEEE Trans. Nucl. Sci. **47**, 337 (2000).
[21]   J. M. Gates*, et al.*, Phys. Rev. C **77**, 034603 (2008).
[22]   K. E. Gregorich*, et al.*, Lawrence Berkeley National Laboratory Report; LBNL-63617 (2007).
[23]   I. Dragojević, K. E. Gregorich, Ch. E. Düllmann, M. A. Garcia, J. M. Gates, S. L. Nelson, L. Stavsetra, R. Sudowe, and H. Nitsche, In preparation (2008).
[24]   K. H. Schmidt, Eur. Phys. J. A **8**, 141 (2000).
[25]   F. P. Heßberger (private communication).

Table I: Experimental conditions and results for the ^{208}Pb(^{51}V,xn)$^{259-x}$Db reaction

Beam energy (MeV)	Excitation energy (MeV)	ε_{BGS}	Observed number of 1n events	1n cross section (pb)	Observed number of 2n events	2n cross section (pb)
236.1	13.1	0.64	1	230^{+520}_{-190}	0	<180
239.7	16.0	0.65	7	2070^{+1100}_{-760}	0	<240
244.1	19.5	0.66	9	1000^{+460}_{-330}	5	250^{+170}_{-110}
247.2	22.0	0.67	3	570^{+550}_{-310}	20	1660^{+450}_{-370}
250.8	24.9	0.68	0	<590	10	1400^{+600}_{-430}
255.0	28.3	0.69	0	<180	3	130^{+130}_{-70}

Table II: Experimental conditions and results for the ^{209}Bi(^{50}Ti,xn)$^{259-x}$Db reaction

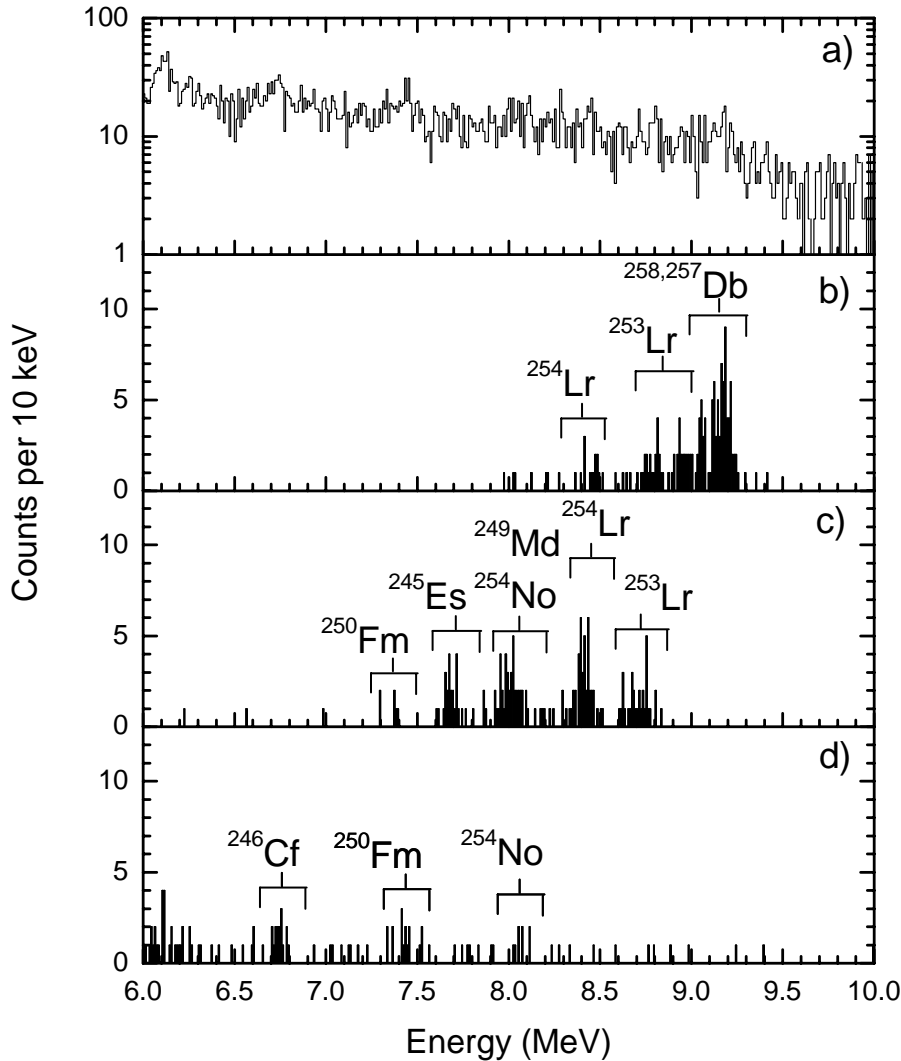| Beam energy (MeV)	Excitation energy (MeV)	ε_{BGS}	Observed number of 1n events	1n cross section (pb)	Observed number of 2n events	2n cross section (pb)
229.5	13.1	0.80	1	55^{+250}_{-45}	0	<140
231.8	15.0	0.81	23	2550^{+720}_{-550}	0	<160
233.6	16.4	0.82	16	5480^{+1730}_{-1370}	0	<280
236.0	18.3	0.83	8	3360^{+1940}_{-1370}	3	650^{+630}_{-350}
238.4	20.3	0.84	9	2600^{+1190}_{-850}	7	890^{+463}_{-330}

FIG. 1. Particle spectra recorded in the focal plane detector for: a) all events from the high-gain spectra anti-coincident with the MWPC and punch-through detectors; b) all α-like events initiating a beam shutoff c) all α-like events occurring during the beam off and correlated within 3σ and 240 s to the α-like event initiating shutoff; d) all α-like events occurring during the beam off that were *not* correlated within 3σ and 240 s to the α-like event initiating beam shutoff. The peaks at 7.4 and 6.7 MeV are due to ^{250}Fm and

^{246}Cf α-particles that are correlated to earlier beam shutoff events. The peak at 8.1 is due to ^{254}No α-decays that are preceded by ^{258}Db α-decays in which the α-particle escaped the front of the detector and imparted only a portion of its energy, thus not triggering a beam shutoff. These decays are long-lived enough to be recorded in subsequent beam shutoffs due to the high rate of Db-like events.
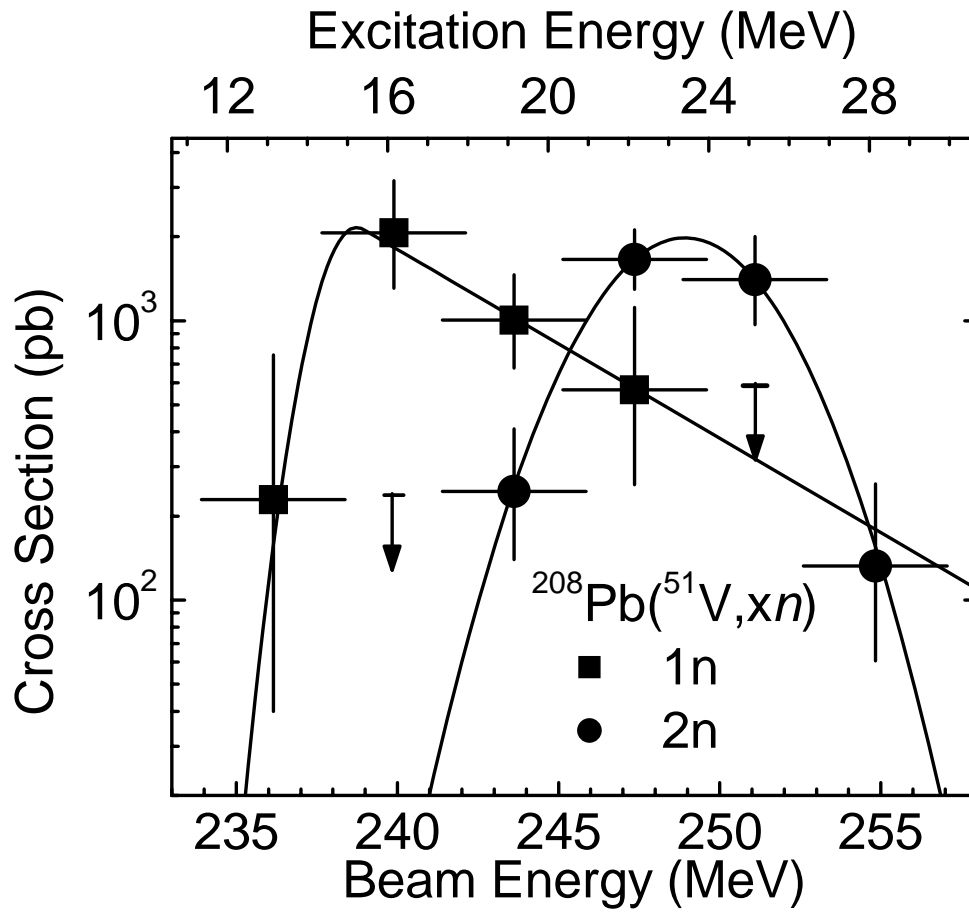
FIG. 2. 1*n* and 2*n* excitation functions for the ^{208}Pb(^{51}V,x*n*)$^{259-x}$Db reactions. Horizontal error bars represent the range of beam energies inside the target. Vertical error bars are uncertainties due to counting statistics. Downward arrows are upper limit cross sections calculated at the 1σ level. The lines are fits to the data using the procedure described in Section III.D and [22, 23].
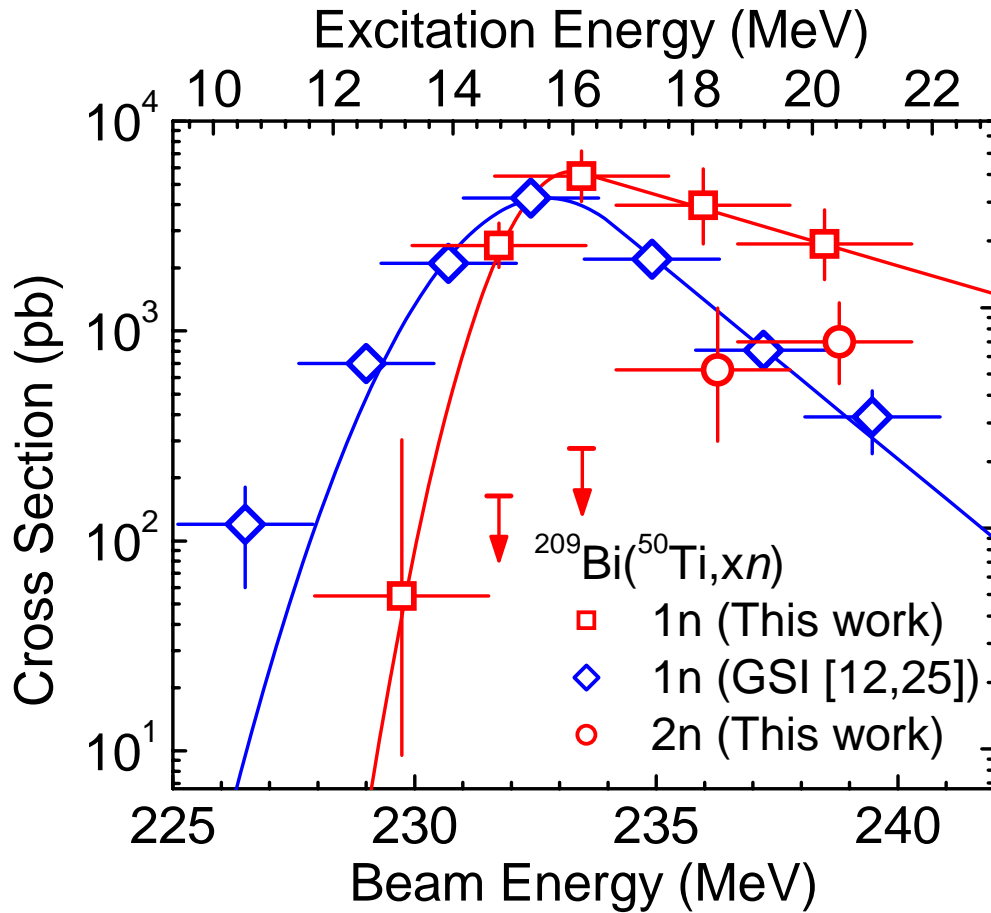
FIG. 3. (Color online) Excitation functions for the ^{209}Bi(^{50}Ti,n)^{258}Db reaction as measured by LBNL (this work) and GSI ([12, 25]). A partial excitation function measured at LBNL for the 2n exit channel is also included. Horizontal error bars represent the range of beam energies inside the target. Vertical error bars are uncertainties due to counting statistics. Downward pointing arrows are upper limit cross sections calculated at the 1σ level. The lines are a Gaussian smoothly joined up to an exponential on the high energy side best fitting the 1n data using the procedure described in Section III.D and [22, 23].
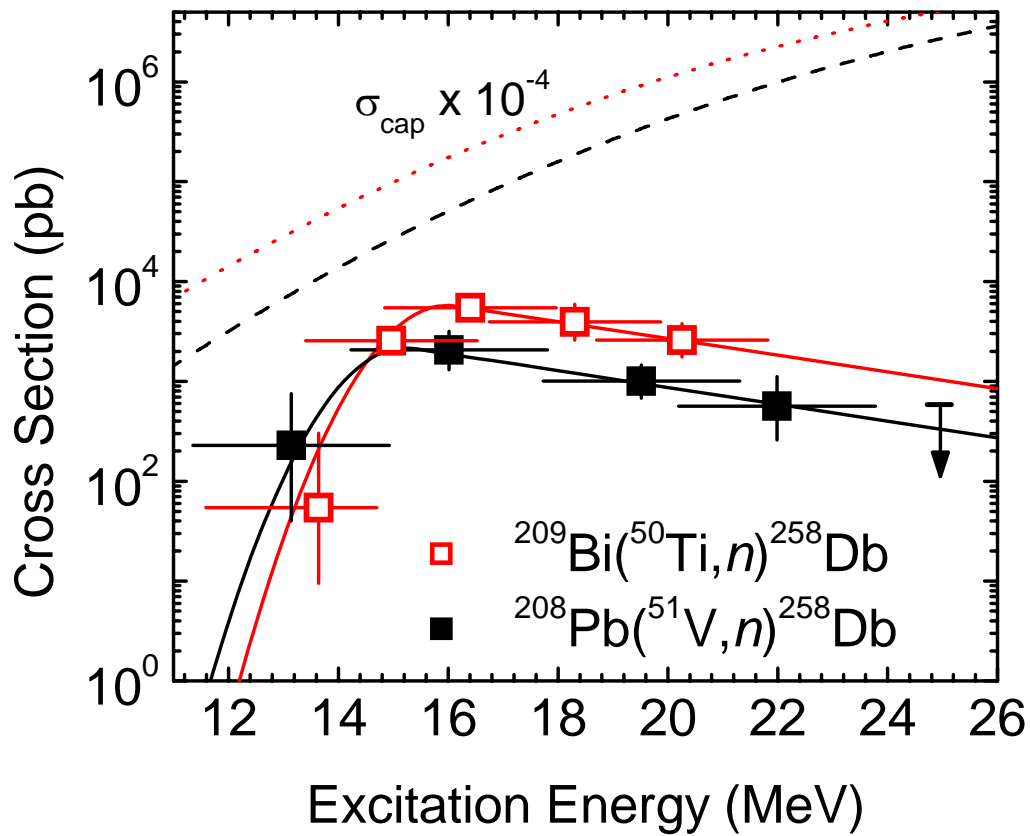
FIG. 4. (Color online) Comparison of the $1n$ excitation functions for the ^{208}Pb(^{51}V,n) and ^{209}Bi(^{50}Ti,n) reactions. Horizontal error bars represent the range of beam energies inside the target. Vertical error bars are uncertainties due to counting statistics. Downward pointing arrows are upper limit cross sections calculated at the 1σ level. The solid lines are Gaussians smoothly joined to exponentials on the high energy side using the procedure described in Section III.D and [22, 23]. The lines are $\sigma_{cap} \times 10^{-4}$ for the ^{208}Pb(^{51}V,n) (dashed) and ^{209}Bi(^{50}Ti,n) (dotted) reactions.
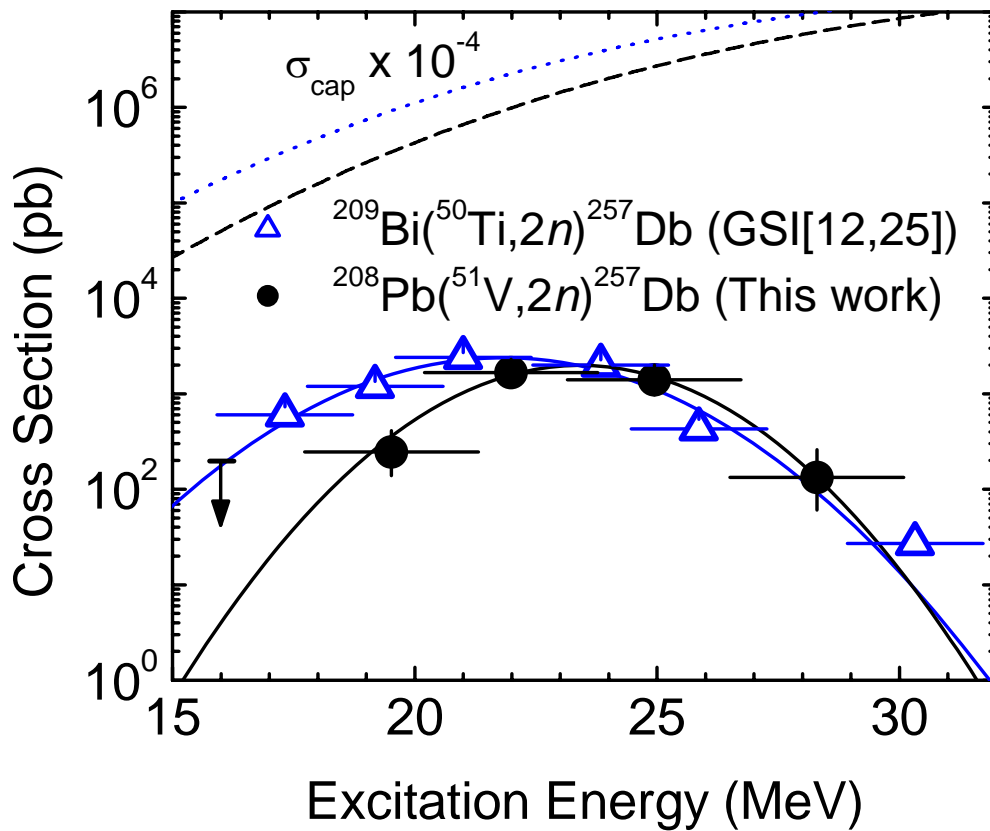
FIG. 5. (Color online) Comparison of the 2*n* excitation functions for the ^{208}Pb(^{51}V,2*n*) (this work) and ^{209}Bi(^{50}Ti,2*n*) [12, 25] reactions. Horizontal error bars represent the range of beam energies inside the target. Vertical error bars are uncertainties due to counting statistics. Downward pointing arrows are upper limit cross sections calculated at the 1σ level. The solid lines are fits to the data using the procedure described in Section III.D and [22, 23]. The broken lines are $\sigma_{cap} \times 10^{-4}$ for the ^{208}Pb(^{51}V,*n*) (dashed) and ^{209}Bi(^{50}Ti,*n*) (dotted) reactions.